

## Comparison of hot electron transport properties in wurtzite phase of ZnS, GaN and 6H-SiC

H. Arabshahi

Physics Department, Ferdowsi University of Mashhad, Mashhad, Iran  
arabshahi@um.ac.ir

### Abstract

An ensemble Monte Carlo simulation have been carried out to study temperature and doping dependencies of electron drift velocity in ZnS, GaN and 6H-SiC. We study how electrons, initially in thermal equilibrium, drift under the action of an applied electric field within bulk of these materials. Calculations are made using a non-parabolic effective mass energy band model, Monte Carlo simulation that includes all of the major scattering mechanisms. The band parameters used in the simulation are extracted from optimized pseudopotential band calculations to ensure excellent agreement with experimental information and ab-initio band models. For all materials, it is found that electron velocity overshoot only occurs when the electric field is increased to a value above a certain critical field, unique to each material. This critical field is strongly dependent on the material parameters. Transient velocity overshoot has also been simulated, with the sudden application of fields up to  $600 \text{ kV m}^{-1}$ , appropriate to the gate-drain fields expected within an operational field effect transistor. The electron drift velocity relaxes to the saturation value of about  $1.5 \times 10^5 \text{ ms}^{-1}$  within 3 ps, for all crystal structures.

**Keywords:** Ensemble Monte Carlo, drift velocity, transient velocity, pseudopotential.

### Introduction

Recent improvements in material quality and contact technology for GaN, ZnS and 6H-SiC-based materials system have led to a rapid progress in devices. These devices include blue-green lasers, blue, green, and amber Light Emitting Diodes, Ultraviolet (UV) photodetectors, and Heterostructure Field Effect Transistors. Wide band gap, high peak and saturation velocities, high breakdown voltage and chemical inertness make GaN, ZnS and 6H-SiC based semiconductors an excellent material for solar-blind optoelectronics, and high-power, hightemperature electronics. These materials are usually grown in the [0001] direction (when they have the wurtzite crystal structure) and in the [111] direction (when they have the zinc blende crystal structure). These are polar axes, and, therefore, these materials exhibit strong lattice polarization effects. These effects are uniquely suited for applications in high temperature piezoelectronics and for applications in pyroelectric sensors.

It is evident that in high temperatures the wide band-gap semiconductors like GaN, ZnS and 6H-SiC have much lower intrinsic carrier concentrations than Si and GaAs (Betazzi *et al.*, 2007). This implies that devices for higher temperatures should be fabricated from wide band-gap semiconductors to avoid the effects of thermally generated carriers (Furno *et al.*, 2008). Also, the wide band-gap semiconductors are of potential interest as a suitable material for high power electronics and because of their direct band gap are benefit for optoelectronic devices, too. ZnO has recently received much attention because of its potential advantages over GaN, including commercial availability of bulk single crystals, amenability

to wet chemical etching and a large exciton binding energy (60 meV, compared with 25 meV for GaN) that causes excitonic emission at room and higher temperatures. Although, the excellent radiation hard characteristics, make ZnO a suitable candidate for space applications (Ozgur *et al.*, 2005).

### Simulation model

Our ensemble Monte Carlo simulations of electron transport in wurtzite GaN, ZnS and 6H-SiC are similar to those of Arabshahi *et al.* [8-9]. As indicated earlier, a three-valley model for the conduction band is employed. In order to calculate the electron drift velocity for large electric fields, consideration of conduction band satellite valleys is necessary. The first-principles band structure of wurtzite crystal structure predicts a direct band gap located at the  $\Gamma$  point and lowest energy conduction band satellite valleys at the  $U$  point and at the  $K$  point. In our Monte Carlo simulation, the  $\Gamma$  valley, the six equivalent  $U$  valleys, the three equivalent  $K$  valleys, are represented by ellipsoidal, non-parabolic dispersion relationships of the following form [10-12]

$$E(k)[1 + \alpha_i E(k)] = \frac{\hbar^2 k^2}{2m^*} \quad (1)$$

where  $m^*$  is effective mass at the band edge and  $\alpha_i$  is the non-parabolicity coefficient of the  $i$ th valley given by Kane model [13] as

$$\alpha_i = \frac{1}{E_g} \left[ 1 - \frac{2m^*}{m_0} \right] \left[ 1 - \frac{E_g \Delta}{3(E_g + \Delta)(E_g + 2\Delta/3)} \right] \quad (2)$$

where  $E_g$  is the band-gap energy and  $\Delta$  is the spin-orbit splitting. We assume that all donors are ionized and that

the free-electron concentration is equal to the dopant concentration. For each simulation, the motion of ten thousand electron particles are examined, the temperature being set to 300 K, and the doping concentration being set to  $10^{17} \text{ cm}^{-3}$ . In the case of the ellipsoidal, non-parabolic conduction valley model, the usual Herring-Vogt transformation matrices are used to map carrier momenta into spherical valleys when particles are drifted or scattered. Electrons in bulk material suffer intravalley scattering by polar optical, non-polar optical and acoustic phonons scattering, intervalley phonons, and ionized impurity scattering.

Acoustic scattering is assumed elastic and the absorption and emission rates are combined under the equipartition approximation, which is valid for lattice temperatures above 77 K. Elastic ionized impurity scattering is described using the screened Coulomb potential of the Brooks-Herring model. Band edge energies, effective masses and non-parabolicities are derived from empirical pseudopotential calculations. Important parameters used throughout the simulations are listed in table 1 (Jacoboni *et al.*, 1989).

Table 1. Important parameters used in the simulations for wurtzite phase ZnO, GaN and SiC (O’Leary *et al.*, 2006)

Material parameters	GaN	ZnS	6H-SiC	
Mass density, $\text{kgm}^{-3}$	6150	5500	3200	
Sound velocity, $\text{ms}^{-1}$	4330	6440	1373	
Static relative permittivity, $\epsilon_0$	9.5	8	9.7	
High frequency relative permittivity, $\epsilon_\infty$	5.35	3.1	6.5	
Acoustic deformation potential, (eV)	8.3	15	15	
Polar optical phonon, $\hbar\omega_{op}$ (meV)	99	66	120	
Direct energy gap, $E_g$ (eV)	3.5	3.1	3.2	
<b>Valley parameters</b>				
	$\Gamma$	U	K	
Electron effective mass ( $m^*/m_0$ )	GaN	0.2	0.33	0.3
	ZnS	0.25	0.43	0.3
	6H-SiC	0.28	0.3	0.54
Nonparabolicity coefficients ( $\text{eV}^{-1}$ )	GaN	0.189	0.054	0.7
	ZnS	0.312	0.045	0.65
	SiC	0.32	0.54	0.03
Valley separation (eV)	GaN	0	2.1	3.1
	ZnS	0	2.4	2.9
	6H-SiC	0	0.6	0.67
Equivalent valley number	1	6.7	2	

**Results**

Fig. 1 shows the simulated velocity-field characteristics of wurtzite zincblende GaN, ZnS and 6H-SiC semiconductors at 300 K, with a background doping concentration of  $10^{17} \text{ cm}^{-3}$ , and with the electric field applied along the c-axes. The simulations suggest that the peak drift velocity for wurzute GaN is  $3.1 \times 10^5 \text{ ms}^{-1}$ , while that for ZnS, and 6H-SiC are about  $\sim 2.2 \times 10^5 \text{ ms}^{-1}$ ,

$2.2 \times 10^5 \text{ ms}^{-1}$  and  $3 \times 10^5 \text{ ms}^{-1}$ , respectively. At higher electric fields, intervalley optical phonon emission dominates, causing the drift velocity to saturate at around  $1.3 \times 10^5 \text{ ms}^{-1}$  for all materials.

For GaN the peak velocity is larger and occurs at lower electric field that is because of its lower effective mass in  $\Gamma$  valley. As the effective mass of the electrons in the upper valleys is greater than that in the lowest valley, the electron in the upper valleys will be slower. As more electrons transfer to the upper valleys, the electron drift velocity decreases (Farahmand *et al.*, 2001).

This leads the negative differential mobility in Fig. 1 for ZnS and GaN. The other important things that is seen in Fig. 1 is dependence of drift velocity on electric field in ZnS and GaN presents a dual-slope behaviour before the peak velocity which may be traced back to the onset of polar optical scattering. The steady-state electron drift velocity versus electric field has been calculated for these materials at different temperatures and various doping concentrations that are seen in Fig. 2 and Fig. 3. It can be seen in Fig.2 that the temperatur increasing causes the drift velocity decreasing. Because the temperature increasing increases the acoustic phonon scattering and impurity scattering, so the electron mobility and drift velocity decreases (Moglestue, 1993). On the other hand the peak velocity occurs in the higher electric fields when the temperature increases. It is interesting that for 6H-SiC the negative differential mobility is observed in low temperature so it may be seen in higher temperature too but in higher electric fields. Fig.3 shows the various dopping concentration do not have considerable effect on the drift velocity.

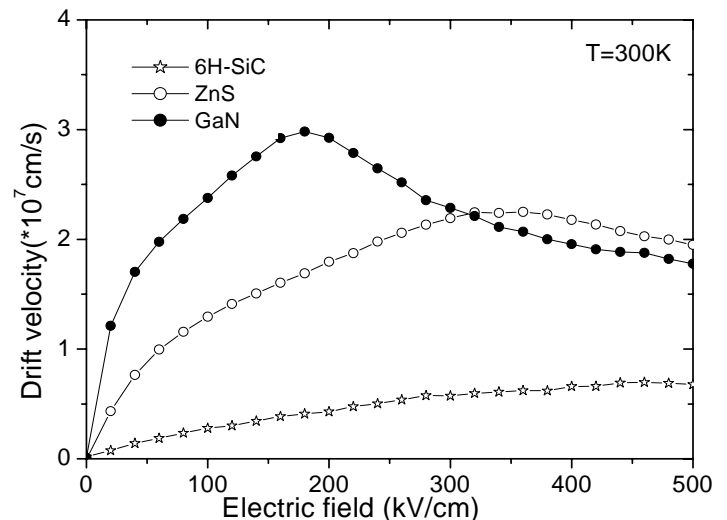


Fig. 1. Calculated electron drift velocity in wurtzite ZnS, GaN and 6H-SiC at T=300 K and  $10^{23} \text{ m}^{-3}$  impurity concentration.

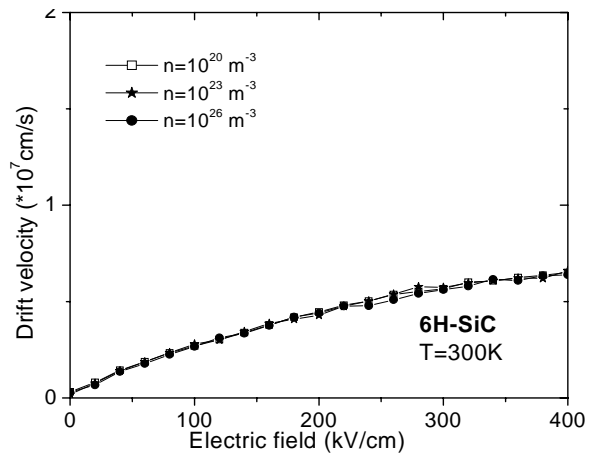
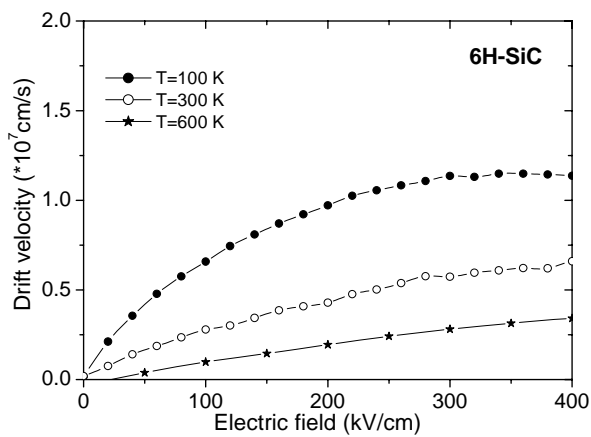
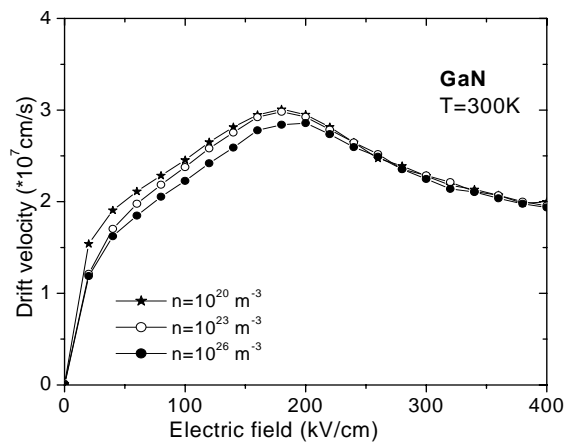
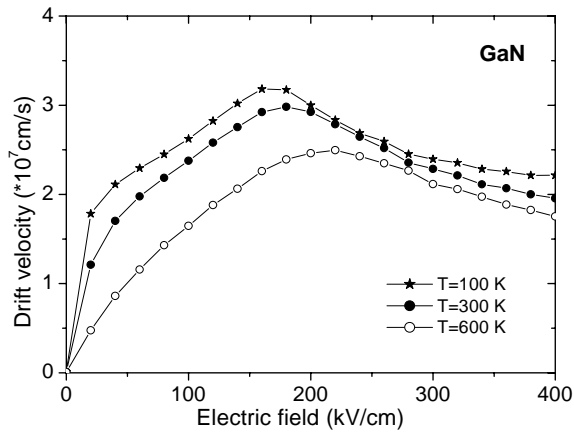
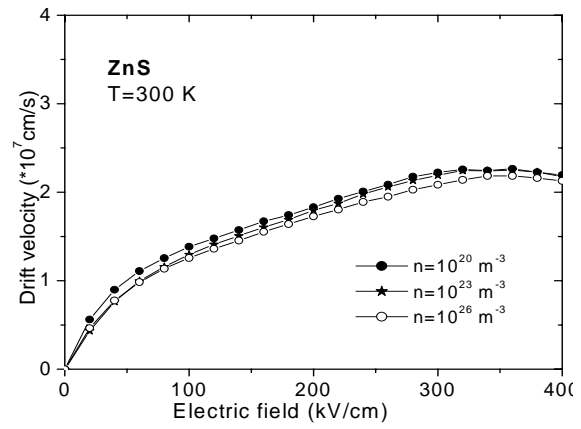
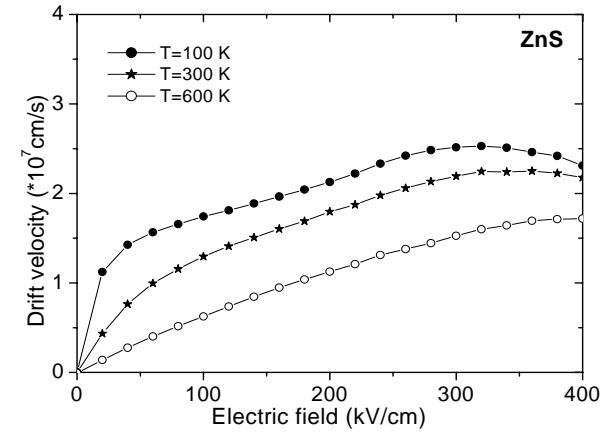


Fig.2. Calculated electron drift velocity in wurtzite ZnS, GaN and 6H-SiC at  $10^{23} \text{ m}^{-3}$  impurity concentration and different temperatures.

Fig.3. Calculated electron drift velocity in wurtzite ZnS, GaN and 6H-SiC at T=300 K and different impurity concentrations.

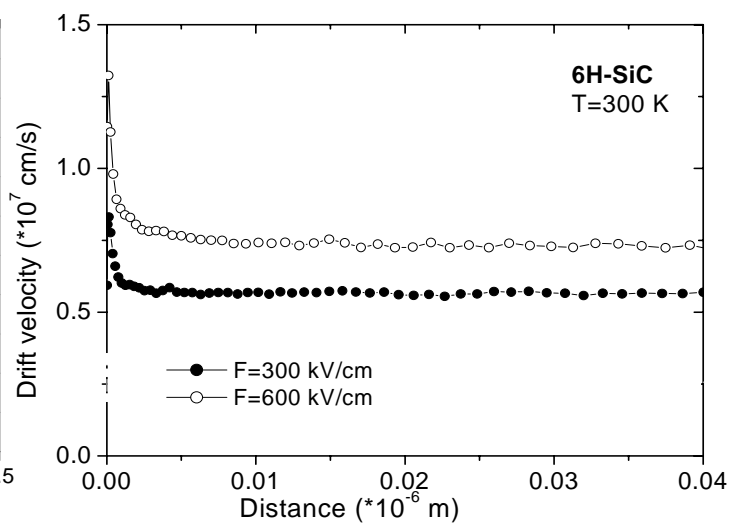
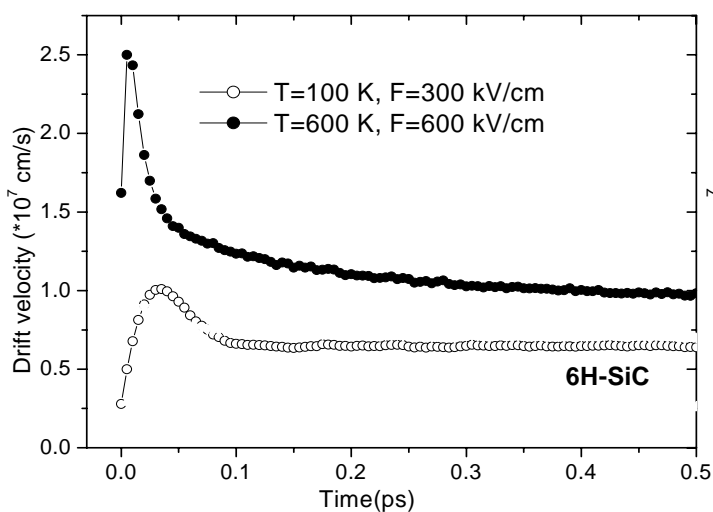
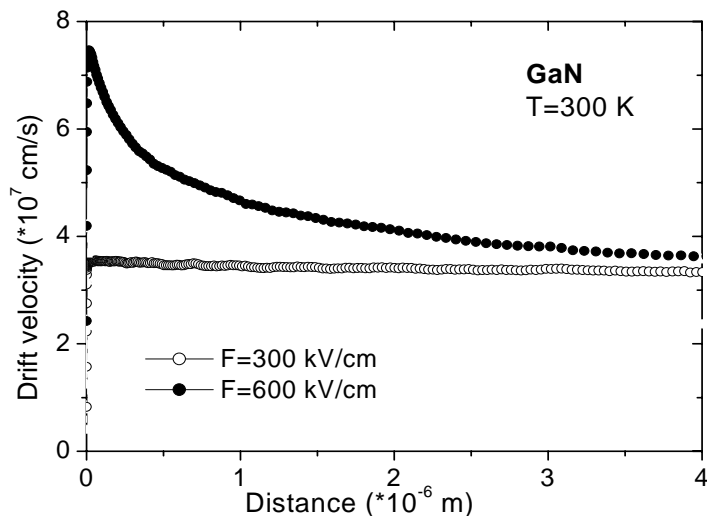
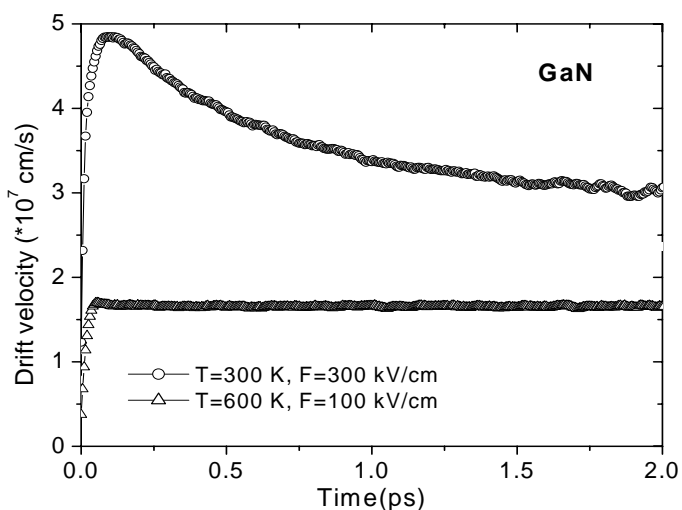
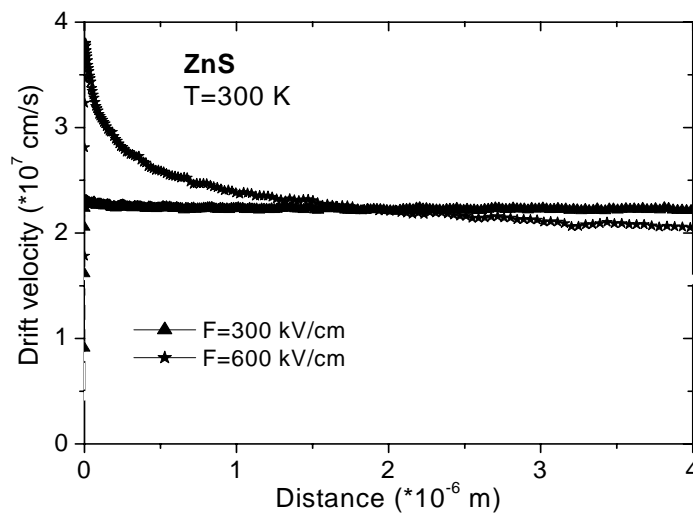
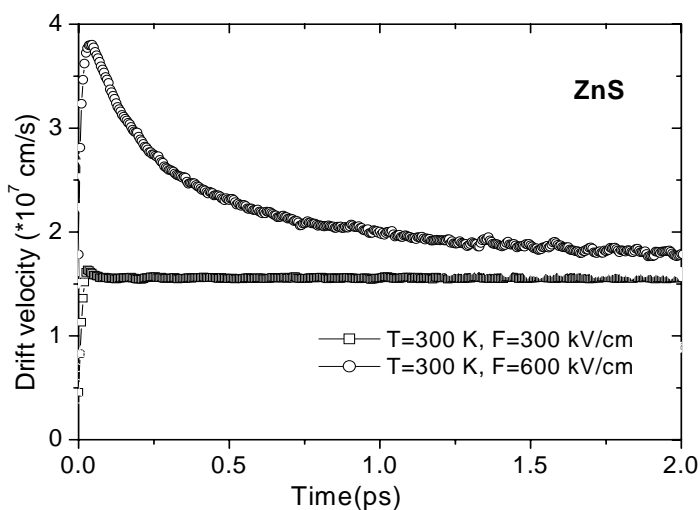


Fig.4. The calculated time evolution of the electron drift velocity in wurtzite ZnS, GaN and 6H-SiC for different values of the electric fields and temperature.

Fig. 5. The calculated distance evolution of the electron drift velocity in wurtzite ZnS, GaN and 6H-SiC at T=300 K for different values of the electric fields.

Because the scattering of ionized impurity is dominated in low temperatures, so the drift velocity does not affect of changing the doping concentration in room temperature (Alberchat *et al.*, 1999).

### Transient electron transport

We have also examined transient electron transport in bulk GaN, ZnS and 6H-SiC semiconductors. The transient response of electrons in these materials are compared in figure 4 and 5 for fields up to  $600 \text{ kV m}^{-1}$  strengths. In GaN, we find very little or no overshoot occurs below the threshold field of  $300 \text{ kV m}^{-1}$ . As the electric field strength is increased to a value above the threshold field, overshoot begins to occur. As the field strength is increased further, both the peak overshoot velocity increases and the time for overshoot relaxation decreases. Fig.5 shows the transient behaviour simulated in ZnS, GaN and 6H-SiC. In ZnS and GaN, for the applied electric field lower than the threshold field electron drift velocity reaches steady-state very quickly with little or no velocity overshoot. In contrast, for applied electric field that are larger than threshold field, transient electron drift velocity shows a significant overshoot. In low electric fields the most of electrons are in central valley with lower effective mass, so the scattering rate is low and transient drift velocity reaches steady-state quickly. But by increasing the applied electric field electrons can gain more energy and by pass the time they could go to the upper valley (O'Leary *et al.*, 2006). In upper valleys, electron effective mass is larger and it causes the scattering rate increases, too. When the scattering rate increases the drift velocity decreases and an overshoot occurs. If applied electric field become more larger, because the electron can gain energy of field sooner the overshoot occurs sooner, too. In 6H-SiC, because the valley separations are lower than ZnS and GaN, the overshoot occurs very soon. But because the electron effective mass in its  $\Gamma$  valley are larger than ZnS and GaN, the drift velocity peak magnitude is lower.

Transient behaviour dependence on temperature are shown in Fig. 5 for two applied electric field, one of them is lower than threshold field and another is larger than threshold field. It can be seen for constant electric field, when temperature increases like the steady-state situation because of increasing scattering rate, drift velocity decreases but the time behaviour is independent of temperature.

### Conclusions

Electron transport at 300 K in bulk wurtzite GaN, ZnS and 6H-SiC have been simulated using an ensemble Monte Carlo simulation. Using valley models to describe the electronic band structure, calculated velocity-field characteristics are in fair agreement with other calculations. Saturation drift velocities  $\sim 1.2 \times 10^5 \text{ ms}^{-1}$

match recent measurements on low-doped bulk samples. The velocity-field characteristics of the materials show similar trends, reflecting the fact that all the semiconductors have satellite valley effective densities of states several times greater than the central  $\Gamma$  valley.

### Acknowledgments

The author thanks Mrs. Maryam Ghovani for writing up the manuscript.

### References

1. Albrecht J D, Ruden P P, Limpijumngong S, Lambrecht W R and Brennan K F, (1999), High field electron transport properties of bulk ZnO, *J. Appl. Phys.* 86, 6864-6869.
2. Arabshahi H, (2009), Comparison of SiC and ZnO field effect transistors for high power applications, *Modern Phys. Lett. B*, 23, 2533-2538.
3. Arabshahi H, (2009), Potential performance of SiC and GaN based metal semiconductor field effect transistors, *Brazilian J. Phys.* 39, 35-38.
4. Bertazzi F, Goano M and Bellotti E, (2007), Electron and hole transport in bulk ZnO: A full band monte carlo study, *J. Elec. Mat.* 36, 857-862.
5. Farahmand M, Garetto C, Bellotti E, Brennan K F, Goano M, Ghillino E, Ghione G, Albrecht J D and Ruden P, (2001), Monte Carlo simulation of electron transport in the III-nitride wurtzite phase materials system: binaries and ternaries, *IEEE Transactions on Electron Devices*, 48, 535-541.
6. Furno E, Bertazzi F, Goano M, Ghione G and Bellotti E, (2008), Hydrodynamic transport parameters of wurtzite ZnO from analytic- and full-band Monte Carlo simulation, *Solid-State Electronics*, 52, 1796-1983.
7. Jacoboni C and Lugli P, (1989), The Monte Carlo method for semiconductor and device simulation, Springer-Verlag.
8. Moglestue C, (1993), Monte Carlo simulation of semiconductor devices, Chapman & Hall.
9. O'Leary S K, Foutz B F, Shur M S and Eastman L, (2006), Steady-state and transient electron transport within the III-V nitride semiconductors, GaN, AlN, and InN: A review, *J. Mater. Sci.: Mater. Electron.* 17, 87-92.
10. Özgür U, Alivov Y, Liu C, Teke A, Reshchikov M A, Doğan S, Avrutin V, Cho S J and Morkoc H, (2005), A comprehensive review of ZnO materials and devices, *J. Appl. Phys.* 98, 041301-1.